

Chemical Science

Accepted Manuscript



This is an *Accepted Manuscript*, which has been through the Royal Society of Chemistry peer review process and has been accepted for publication.

Accepted Manuscripts are published online shortly after acceptance, before technical editing, formatting and proof reading. Using this free service, authors can make their results available to the community, in citable form, before we publish the edited article. We will replace this *Accepted Manuscript* with the edited and formatted *Advance Article* as soon as it is available.

You can find more information about *Accepted Manuscripts* in the [Information for Authors](#).

Please note that technical editing may introduce minor changes to the text and/or graphics, which may alter content. The journal's standard [Terms & Conditions](#) and the [Ethical guidelines](#) still apply. In no event shall the Royal Society of Chemistry be held responsible for any errors or omissions in this *Accepted Manuscript* or any consequences arising from the use of any information it contains.



www.rsc.org/chemicalscience



In situ small-angle X-ray scattering studies of sterically-stabilized diblock copolymer nanoparticles formed during polymerization-induced self-assembly in non-polar media

Received 00th January 20xx,
Accepted 00th January 20xx

DOI: 10.1039/x0xx00000x

www.rsc.org/

Matthew J. Derry,^{*a} Lee A. Fielding,^{a,b} Nicholas J. Warren,^a Charlotte J. Mable,^a Andrew J. Smith,^c Oleksandr O. Mykhaylyk^{*a} and Steven P. Armes^{*a}

Reversible addition-fragmentation chain transfer (RAFT) dispersion polymerization of benzyl methacrylate (BzMA) is utilized to prepare a series of poly(stearyl methacrylate)-poly(benzyl methacrylate) (PSMA-PBzMA) diblock copolymer nano-objects at 90 °C directly in mineral oil. Polymerization-induced self-assembly (PISA) occurs under these conditions, with the resulting nanoparticles exhibiting spherical, worm-like or vesicular morphologies when using a relatively short PSMA₁₃ macromolecular chain transfer agent (macro-CTA), as confirmed by transmission electron microscopy (TEM) and small-angle X-ray scattering (SAXS) studies. Only kinetically-trapped spherical nanoparticles are obtained when using longer macro-CTAs (e.g. PSMA₁₈ or PSMA₃₁), with higher mean degrees of polymerization (DPs) for the PBzMA core-forming block producing progressively larger spheres. SAXS is used for the first time to monitor the various morphological transitions that occur *in situ* during the RAFT dispersion polymerization of BzMA when targeting either spheres or vesicles as the final copolymer morphology. This powerful characterization technique in combination with ¹H NMR studies enables the evolution of particle diameter, mean aggregation number, number of copolymer chains per unit surface area (S_{agg}) and the distance between adjacent copolymer chains at the core-shell interface (d_{int}) to be monitored as a function of monomer conversion for kinetically-trapped spheres. Moreover, the gradual evolution of copolymer morphology during PISA is confirmed unequivocally, with approximate 'lifetimes' assigned to the intermediate pure sphere and worm morphologies when targeting PSMA₁₃-PBzMA₁₅₀ vesicles. Within vesicle phase space, the membrane thickness (T_m) increases monotonically with PBzMA DP. Furthermore, a combination of dynamic light scattering (DLS), TEM and *post mortem* SAXS studies indicate that the lumen volume is reduced while the overall vesicle dimensions remain essentially constant. Thus the constrained vesicles grow inwards, as recently reported for an aqueous PISA formulation. This suggests a universal vesicle growth mechanism for all PISA formulations.

Introduction

It has been known for more than fifty years that diblock copolymers self-assemble into well-defined nanoparticles when dispersed in a selective solvent for one of the blocks.¹⁻⁴

For example, there is a vast range of literature describing the micellar self-assembly of polystyrene-based block copolymers in non-polar media: spherical morphologies are obtained in most cases,⁵⁻¹¹ but examples of worm-like (or cylindrical)⁹⁻¹³ and vesicular¹¹ morphologies have also been reported. More recently, metal-containing diblock copolymers have been utilized for the formation of cylindrical micelles in *n*-alkanes.¹⁴⁻¹⁶ The commercial potential for diblock copolymer nanoparticles dispersed in non-polar solvents was highlighted by Zheng *et al.*, who reported that spherical nanoparticles of approximately 40 nm diameter offer enhanced boundary lubrication performance when dispersed in base oil.¹⁷ Moreover, self-assembled block copolymer nanoparticles have been shown to act as effective dispersants for diesel soot, which in turn minimizes wear and hence improves engine efficiency and long-term performance.^{18,19}

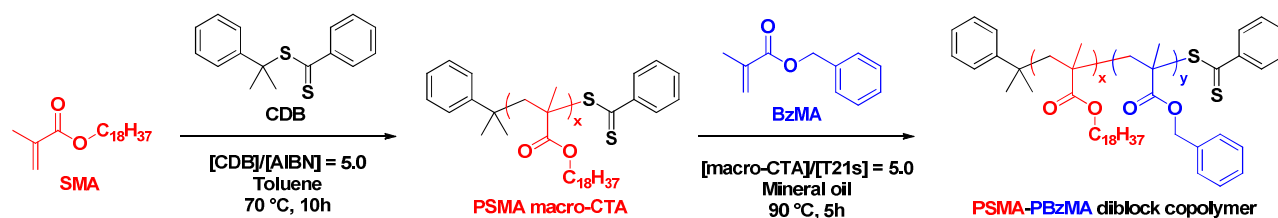
Recently, there has been considerable interest in the development of polymerization-induced self-assembly (PISA), particularly using reversible addition-fragmentation chain

^a Dainton Building, Department of Chemistry, The University of Sheffield, Brook Hill, Sheffield, South Yorkshire, S3 7HF, UK. E-mail: s.p.arnes@sheffield.ac.uk; o.mykhaylyk@sheffield.ac.uk; m.derry@sheffield.ac.uk

^b Present address: The School of Materials, The University of Manchester, Oxford Road, Manchester, M13 9PL, UK.

^c Diamond Light Source Ltd., Diamond House, Harwell Science and Innovation Campus, Didcot, Oxfordshire, OX11 0DE, UK.

† Electronic Supplementary Information (ESI) available: Experimental details including *in situ* SAXS measurements; Synthesis and characterization of (co)polymers; Kinetic study for the synthesis of a PSMA₃₁ macro-CTA; Data modelling for *in situ* SAXS experiments including kinetic renormalization, determination of BzMA monomer within the nanoparticle cores and estimation of the standard deviation in the molecular weight distribution; Example 2D SAXS patterns; TEM images of octopi and jellyfish; DLS, TEM and SAXS analyses of PSMA₁₃-PBzMA_x vesicles; SAXS models used for spherical micelles and vesicles. See DOI: 10.1039/x0xx00000x



Scheme 1 Synthesis of a poly(stearyl methacrylate) (PSMA) macro-CTA via RAFT solution polymerization in toluene at 70 °C, followed by RAFT dispersion polymerization of benzyl methacrylate (BzMA) in mineral oil at 90 °C.

transfer (RAFT)²⁰⁻²² dispersion polymerization.²³⁻²⁷ PISA provides an efficient and versatile route to diblock copolymer nanoparticles directly at high solids without the need for post-polymerization processing, making this approach amenable to scale-up.²⁸ Most of the PISA literature has focused on optimizing aqueous^{26, 29-40} or alcoholic⁴¹⁻⁵³ formulations. In contrast, there are relatively few examples of suitable PISA formulations conducted in non-polar solvents such as *n*- or *iso*-alkanes.⁵⁴⁻⁶² Charleux and co-workers evaluated dithiobenzoate and trithiocarbonate RAFT chain transfer agents (CTAs) for the polymerization of methyl acrylate in *iso*-dodecane.^{54, 55} However, broad molecular weight distributions and low blocking efficiencies (i.e. inefficient re-initiation of the macro-CTA) were achieved, suggesting rather poor control. Fielding *et al.*⁵⁷ reported reasonably well-controlled RAFT polymerizations for the synthesis of poly(lauryl methacrylate)-poly(benzyl methacrylate) (PLMA-PBzMA) diblock copolymer nanoparticles in *n*-heptane via PISA. In this case, either spheres, worms or vesicles could be obtained provided that the PLMA stabilizer block was sufficiently short to enable efficient sphere-sphere fusion to occur during PISA. The construction of a phase diagram facilitated reproducible targeting of the worm phase, with these highly anisotropic nanoparticles forming free-standing gels in *n*-heptane at 20 °C.⁵⁷ Derry *et al.*²⁸ recently revisited this RAFT dispersion polymerization formulation, where a highly convenient ‘one-pot’ protocol was developed for the synthesis of PLMA-PBzMA spheres in mineral oil at high solids content. This work highlighted the potential industrial relevance of such PISA formulations.

Small-angle X-ray scattering (SAXS) techniques have been employed to characterize nanoparticle morphologies obtained by various PISA formulations.^{38, 48, 58, 62-70} In particular, thermally-induced micelle-to-unimer^{64, 65} and worm-to-sphere^{58, 64, 65} transitions have been studied, as well as the evolution of vesicle dimensions on increasing the mean degree of polymerization (DP) of the core-forming block.⁶⁷ Most notably for non-polar formulations, heating a free-standing PLMA-PBzMA worm gel in *n*-dodecane to 160 °C resulted in the formation of a free-flowing dispersion of spheres.⁵⁸ This change in copolymer morphology was attributed to ingress of hot solvent leading to surface plasticization of the core-forming PBzMA block, as indicated by variable-temperature ¹H NMR studies. Such solvation lowers the packing parameter³⁰ and hence drives the worm-to-sphere transition, which was confirmed by transmission electron microscopy (TEM) studies.⁵⁸ SAXS was particularly useful for characterizing this

specific formulation, since the reduction in the mean worm contour length (L_w) could be monitored on heating from 20 °C ($L_w \approx 600$ nm) to 90 °C ($L_w \approx 350$ nm), with spherical nanoparticles of ~17 nm diameter being observed at 160 °C. In related work, Lowe and co-workers used TEM and dynamic light scattering (DLS) to demonstrate a worm-to-sphere transition for PSMA-PPMA nanoparticles in *n*-tetradecane⁵⁹ and *n*-octane,⁶¹ with ¹H NMR spectroscopy confirming a similar surface plasticization effect for the core-forming PPPMA block on heating to 95 °C. Recently, SAXS has been utilized to characterize microphase separation within block copolymer microparticles,⁷¹ with time-resolved studies being conducted during the synthesis of poly(methyl methacrylate)-poly(benzyl methacrylate) (PMMA-PBzMA) block copolymers via RAFT dispersion polymerization in supercritical CO₂.⁷²

Herein we report the PISA synthesis of poly(stearyl methacrylate)-poly(benzyl methacrylate) (PSMA-PBzMA) diblock copolymer nano-objects directly in mineral oil (see Scheme 1). We demonstrate that PSMA offers significant advantages over PLMA in terms of both blocking efficiency and control during the RAFT dispersion polymerization of BzMA. A detailed phase diagram is constructed for this new dispersion polymerization formulation using TEM, while DLS and SAXS are utilized to characterize the nanoparticle dispersions. In particular, we utilize a synchrotron source to conduct SAXS studies of the *in situ* evolution of the copolymer morphology during PISA. SAXS provides remarkably detailed insights regarding the sphere-to-worm and worm-to-vesicle transitions during this non-aqueous PISA formulation and also sheds light on the mechanism of *in situ* vesicle growth.

Results and discussion

Synthesis of macro-CTAs

RAFT solution polymerization of stearyl methacrylate (SMA) was conducted in toluene at 70 °C using cumyl dithiobenzoate (CDB) as a CTA. Three PSMA macro-CTAs were characterized using ¹H NMR spectroscopy and the mean degree of polymerization (DP) was calculated to be 13, 18 or 31 (see Supporting Information, Table S1). Each homopolymerization was quenched at 72%-76% conversion in order to avoid monomer-starved conditions, thus ensuring the retention of RAFT end-groups.^{73, 74} This is usually required for high blocking efficiencies and hence well-defined PSMA-PBzMA diblock copolymers. Each PSMA macro-CTA had a polydispersity (M_w/M_n) of ≤ 1.24 , which is consistent with previous studies

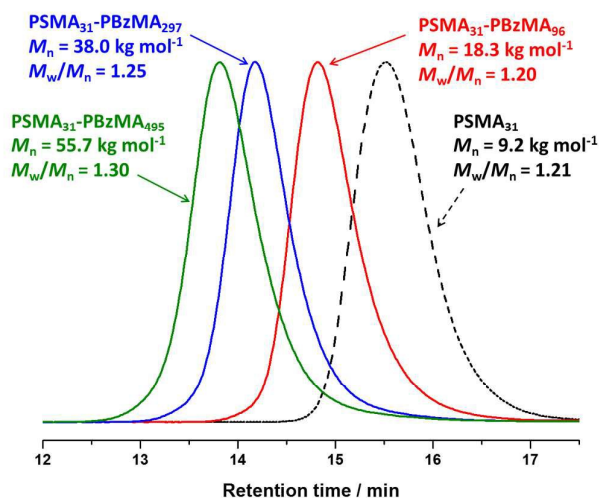


Fig. 1 THF gel permeation chromatograms (vs. poly(methyl methacrylate) standards) obtained for three PSMA₃₁-PBzMA_x diblock copolymers prepared via RAFT dispersion polymerization of BzMA in mineral oil at 90 °C at 20% w/w solids. The precursor PSMA₃₁ macro-CTA (prepared in toluene at 70 °C at 40% w/w solids; black dashed curve) is also shown as a reference.

reporting well-controlled RAFT syntheses under these conditions.⁵⁷ A typical kinetic study of the synthesis of a PSMA₃₁ macro-CTA via RAFT solution polymerization was conducted (Figure S3a). After an initial induction period, first-order kinetics were observed prior to quenching at 72% conversion after 10 h. Gel permeation chromatography (GPC) analysis indicated a linear evolution of molecular weight with conversion (Figure S3b).

PSMA₁₈-PBzMA_x and PSMA₃₁-PBzMA_x diblock copolymer spheres

BzMA monomer was polymerized using two of the low polydispersity PSMA macro-CTAs (DP = 18, or 31) in turn via RAFT dispersion polymerization (see Supporting Information, Table S2). In all cases, ≥ 97% BzMA conversion was achieved within 5 h at 90 °C, as judged by ¹H NMR spectroscopy. Only spherical morphologies were obtained when using a longer PSMA stabilizer block (DP = 18 or 31). This indicates that the upper limit PSMA DP for access to higher order morphologies (i.e. worms or vesicles) is relatively low for this PISA formulation in mineral oil. Longer PSMA stabilizer blocks confer enhanced steric stabilization, which prevents the efficient 1D fusion of multiple spheres and therefore the formation of anisotropic worms. Similar observations were reported for PLMA-PBzMA diblock copolymers prepared via RAFT dispersion polymerization of BzMA in *n*-heptane,⁵⁷ *n*-dodecane⁵⁸ and mineral oil.²⁸ In these earlier studies, the upper limit PLMA stabilizer DP which allowed access to higher order morphologies was 16-18. Given the relative molecular volumes of the LMA (C₁₂ side-chain) and SMA (C₁₈ side-chain) repeat units, it is reasonable that using PSMA₁₈ only allows access to spheres. Clearly, PSMA₁₃ has a comparable molecular volume to that of PLMA₁₈, which is why using the former macro-CTA allows access to worms and vesicles, as well as spheres.

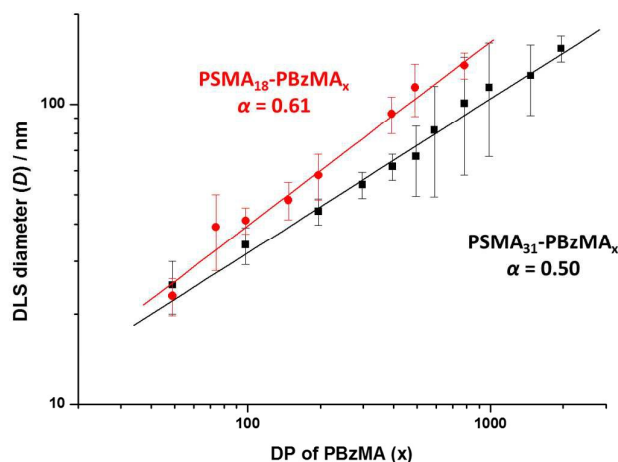


Fig. 2 Relationship between intensity-average sphere diameter (D) and target DP of the PBzMA block (x) for series of PSMA₁₈-PBzMA_x (red circles) and PSMA₃₁-PBzMA_x (black squares) diblock copolymer spheres prepared via RAFT dispersion polymerization of BzMA in mineral oil at 90 °C. The error bars represent the standard deviation of the diameter and α is the scaling factor.

Compared to related RAFT dispersion polymerization syntheses conducted in non-polar media,⁵⁴⁻⁵⁸ the present PSMA-PBzMA formulation enables relatively narrow molecular weight distributions to be obtained even when targeting PBzMA DPs as high as 500, which corresponds to an experimentally determined M_n of ~56 kg mol⁻¹ (Figure 1). GPC analysis of PSMA₃₁-PBzMA_x ($x \leq 500$) diblock copolymers in THF eluent indicates M_w/M_n values ranging between 1.19 and 1.30, which suggests good RAFT control. Also, the unimodal nature of these curves and the clear shift from the original PSMA₃₁ macro-CTA indicates relatively high blocking efficiencies. In contrast, relatively broad molecular weight distributions ($M_w/M_n > 1.50$) were reported by Fielding *et al.* when targeting x values above 300 for PLMA₃₇-PBzMA_x diblock copolymers via closely-related PISA syntheses conducted in *n*-heptane.⁵⁷ However, it is not yet understood why merely using a PSMA macro-CTA instead of a PLMA macro-CTA leads to significantly better pseudo-living character during the dispersion polymerization of BzMA.

A series of spherical nanoparticles with tunable diameters was conveniently prepared in mineral oil at 20% w/w solids simply by varying the target DP of the core-forming PBzMA block when using a PSMA macro-CTA with a sufficiently high DP. For example, PSMA₁₈-PBzMA_x spheres ranging from 23 to 135 nm diameter (as judged by DLS) were obtained when targeting x values of 50 to 800. Similarly, well-defined PSMA₃₁-PBzMA_x spheres of 25 to 154 nm diameter were produced for $x = 50$ to 2000. The mean sphere diameter, D , is related to the mean DP of the core-forming block, x , by a scaling exponent, α , as indicated by the equation $D \sim kx^\alpha$ where k is a constant.^{75, 76} Figure 2 shows double-logarithmic plots of D , as judged by DLS, against x for each series of PSMA₁₈-PBzMA_x and PSMA₃₁-PBzMA_x spheres. A clear relationship is observed in each case, which enables the corresponding scaling exponent (α) to be determined. This parameter provides important information

regarding the behavior of the PBzMA core-forming chains. For the PSMA₃₁-PBzMA_x series we find that $\alpha = 0.50$, which

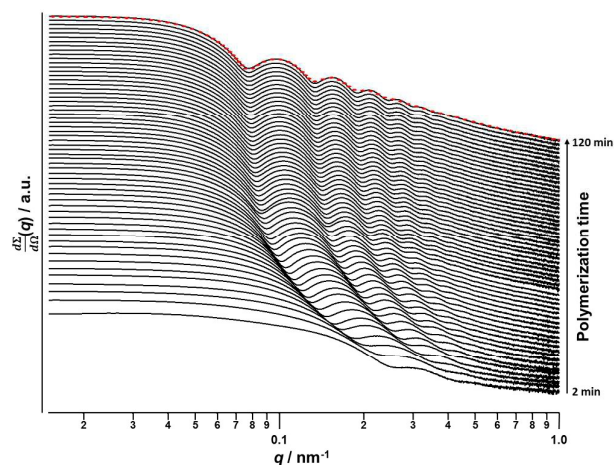


Fig. 3 SAXS patterns obtained *in situ* during the PISA synthesis of PSMA₃₁-PBzMA₂₀₀₀ diblock copolymer spheres at 90 °C in mineral oil at 10% w/w solids. Red dashes indicate the data fit to the final SAXS pattern recorded after 120 min using a spherical micelle model.⁷⁷⁻⁷⁹

corresponds to unperturbed PBzMA chains.^{75, 76, 80} According to the literature, such low α values suggest weak segregation (and minimal solvation).^{75, 76, 80} On the other hand, we find that $\alpha = 0.61$ for the PSMA₁₈-PBzMA_x series, indicating that the PBzMA chains are more stretched and may have a finite degree of solvation. This means that, for a given PBzMA_x block (where $x > 50$), larger spheres are always obtained when using the shorter PSMA₁₈ stabilizer block. For example, DLS studies indicate that spheres obtained when targeting a core-forming PBzMA DP of 400 are larger when using the PSMA₁₈ macro-CTA (93 nm) compared to the PSMA₃₁ macro-CTA (62 nm).

In situ SAXS studies of the PISA synthesis of PSMA₃₁-PBzMA₂₀₀₀ spheres

A synchrotron X-ray source was used to acquire SAXS patterns *in situ* during the PISA synthesis of PSMA₃₁-PBzMA₂₀₀₀ diblock copolymer spheres at 90 °C in mineral oil at 10% w/w solids. The sample cell was a 2 mm glass capillary and scattering patterns were recorded every 2 min for 120 min (Figure 3). The onset of micellization occurs when the growing PBzMA chains become sufficiently long to induce nucleation.^{26, 27} This occurred within around 2 min of the polymerization, as indicated by the presence of a local minimum at $q \sim 0.23 \text{ nm}^{-1}$ (where $q = 4\pi \sin \vartheta / \lambda$ is the length of the scattering vector, λ is the wavelength of X-ray radiation and ϑ is one-half of the scattering angle). The characteristic length scale corresponding to this feature is the mean core radius of the spherical diblock copolymer nanoparticles (R_s), which was observed to be 15 nm. Since the PISA synthesis was conducted at 10% w/w solids, it was necessary to incorporate an appropriate structure factor⁸¹ into a well-known spherical micelle model⁷⁷⁻⁷⁹ in order to obtain satisfactory fits to the SAXS patterns.

Monitoring this minimum as it shifts to lower q (larger radii) as the BzMA polymerization proceeded provides useful information regarding the kinetics of nanoparticle growth. However, in order to fit the SAXS data shown in Figure 3 to a

spherical micelle model,⁷⁷⁻⁷⁹ the *instantaneous BzMA conversion* is required, since this in turn determines the mean

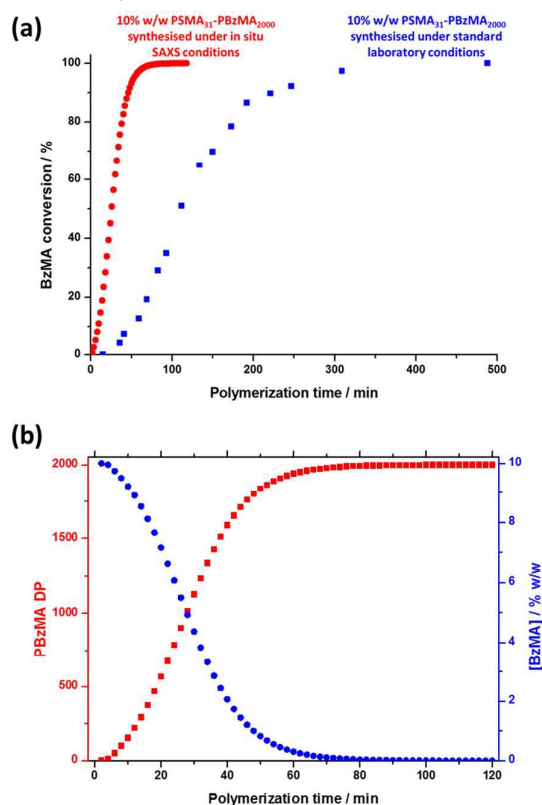


Fig. 4 (a) Conversion vs. time curve (blue squares) for the RAFT dispersion polymerization of BzMA in mineral oil at 90 °C when targeting PSMA₃₁-PBzMA₂₀₀₀ block copolymer spheres at 10% w/w solids using T21s initiator under normal laboratory conditions and the renormalized conversion vs. time curve (red circles) calculated for the same PISA synthesis during *in situ* SAXS studies. (b) Change in the PBzMA DP (red data) and the concentration of BzMA monomer ([BzMA], blue data) during the *in situ* SAXS studies when targeting PSMA₃₁-PBzMA₂₀₀₀ spheres.

DP and hence the molecular volume occupied by a single growing core-forming (PBzMA) block within the sphere [$V_s = (DP_{\text{PBzMA}} \cdot M_{n,\text{BzMA}}) / (N_A \cdot \rho)$], where $M_{n,\text{BzMA}}$ corresponds to the molecular weight of the one BzMA unit within the PBzMA block and ρ is the density of PBzMA). No further change in the SAXS patterns shown in Figure 3 was taken to signify the end of the polymerization. Unfortunately, the BzMA polymerization was complete within 120 min during the *in situ* SAXS studies, whereas around 500 min was required for the same formulation in a typical laboratory-scale synthesis (~20 mL reaction volume) conducted using an oil bath and stirrer hot plate. A possible reason for this significant increase in polymerization rate could be additional radical species generated by the intense X-ray photon flux provided by the synchrotron source.^{82, 83} The ~125 μL reaction volume of the capillary used for the SAXS studies precludes sampling of the polymerizing reaction mixture. Instead, intermediate BzMA conversions were calculated by renormalizing the kinetic data set obtained for the laboratory-scale synthesis. More specifically, a sigmoid function was used to calculate intermediate BzMA conversions (see Figure 4a and

Table 1. Evolution of BzMA conversion, the mean degree of polymerization (DP) of the core-forming PBzMA block, the molecular volume occupied by a single PBzMA chain within the spherical core (V_s), the spherical core diameter ($D_s = 2R_s$), volume fraction of BzMA monomer within the core domain (φ_{BzMA}), mean aggregation number of a sphere (N_s), number of copolymer chains per unit surface area (S_{agg}) and mean distance between adjacent chains at the core-shell interface (d_{int}) during the PISA synthesis of PSMA₃₁-PBzMA₂₀₀₀ diblock copolymer spheres. The standard deviation in D_s ($\sigma_{D_s} = 2\sigma_{R_s}$) and the associated error in V_s , N_s , S_{agg} and d_{int} are indicated.

Time / min	BzMA Conversion / %	PBzMA DP	V_s / nm^3	D_s / nm	φ_{BzMA}	N_s	S_{agg} / nm^{-2}	d_{int} / nm
8	5.0	99	25 ± 2	35 ± 5	0.691	292 ± 28	0.074 ± 0.007	3.7 ± 0.4
10	7.8	155	39 ± 4	42 ± 5	0.586	429 ± 41	0.076 ± 0.007	3.6 ± 0.3
14	14.7	294	73 ± 7	54 ± 5	0.437	633 ± 60	0.069 ± 0.007	3.8 ± 0.4
20	28.4	569	141 ± 13	66 ± 6	0.282	769 ± 73	0.056 ± 0.005	4.2 ± 0.4
28	50.8	1015	252 ± 24	78 ± 6	0.147	845 ± 80	0.044 ± 0.004	4.8 ± 0.5
34	66.8	1335	331 ± 32	88 ± 6	0.083	978 ± 93	0.040 ± 0.004	5.0 ± 0.5
40	79.3	1587	394 ± 37	95 ± 7	0.042	1082 ± 103	0.038 ± 0.004	5.1 ± 0.5
46	87.9	1758	436 ± 41	100 ± 8	0.018	1168 ± 111	0.037 ± 0.004	5.2 ± 0.5
52	93.2	1864	463 ± 44	102 ± 8	0.004	1210 ± 115	0.037 ± 0.003	5.2 ± 0.5
60	97.0	1939	481 ± 46	106 ± 8	0.000	1289 ± 122	0.037 ± 0.003	5.2 ± 0.5
68	98.7	1973	490 ± 47	109 ± 8	0.000	1385 ± 132	0.037 ± 0.004	5.2 ± 0.5
84	99.8	1995	495 ± 47	113 ± 8	0.000	1519 ± 144	0.038 ± 0.004	5.1 ± 0.5
120	100	2000	496 ± 47	117 ± 9	0.000	1688 ± 160	0.039 ± 0.004	5.0 ± 0.5

Supporting Information) since this best described the conversion vs. time curve.⁸⁴ The resulting BzMA conversions were subsequently used to calculate the instantaneous PBzMA DP during the PISA synthesis (see Figure 4b, red data). It must be noted that due to the nature of the renormalization using the sigmoid function, the predicted kinetic data for the *in situ* SAXS measurements are a smooth representation of the somewhat scattered experimental data obtained under standard laboratory conditions.

As expected, the spherical core diameter of the growing nanoparticles (D_s) increases monotonically with polymerization time (see Figure 5a and Table 1). At the end of the BzMA polymerization, at least six minima are visible in the final scattering pattern (120 min, Figure 3), indicating a relatively narrow size distribution for the resulting PSMA₃₁-PBzMA₂₀₀₀ spheres. Data fitting for various SAXS patterns during the RAFT dispersion polymerization of PSMA₃₁-PBzMA₂₀₀₀ spheres indicated essentially no solvent associated with the core-forming PBzMA block, which is consistent with the PSMA₃₁-PBzMA_x data set shown in Figure 2. Moreover, ¹H NMR studies of the latter laboratory-scale syntheses (data not shown) confirmed that the volume fraction of solvent within the core domain (x_{sol}) is essentially zero. Thus, when fitting SAXS patterns recorded during the polymerization, the mean number of copolymer chains per sphere (N_s) was calculated based solely on the volume fraction of BzMA monomer within the core domain (φ_{BzMA}), R_s and V_s as shown below.

$$N_s = (1 - \varphi_{BzMA}) \times \frac{4}{3} \frac{\pi R_s^3}{V_s} \quad (1)$$

Values for φ_{BzMA} were estimated via centrifugation of selected dispersions of PSMA₃₁-PBzMA_x spheres (obtained at full BzMA conversion via laboratory-scale syntheses) to which varying amounts of BzMA monomer and additional mineral oil had been added in order to replicate specific intermediate BzMA

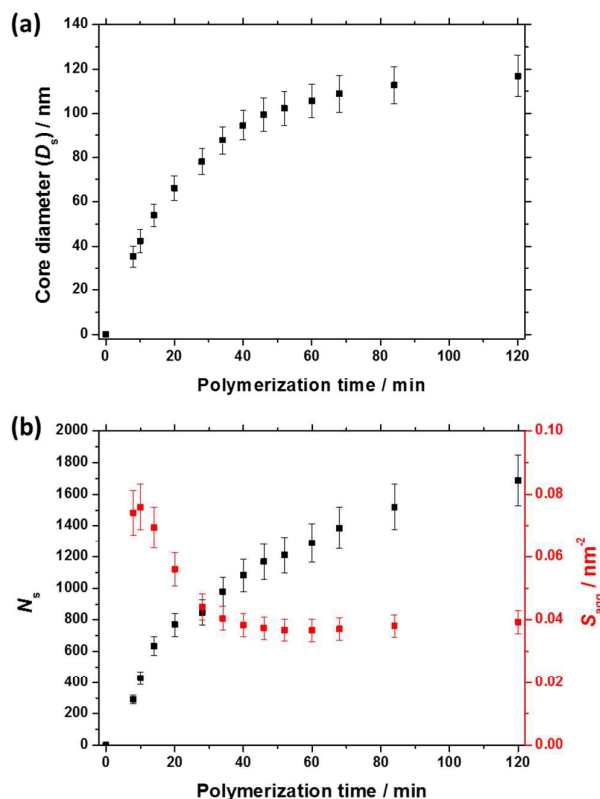


Fig. 5 (a) Evolution of the mean core diameter (D_{co}) and (b) mean aggregation number (N_{agg} , black data set) and number of aggregated chains per unit surface area (S_{agg} , red data set) during the PISA synthesis of PSMA₃₁-PBzMA₂₀₀₀ diblock copolymer spheres, as judged by *in situ* SAXS studies.

conversions during the synthesis of PSMA₃₁-PBzMA₂₀₀₀ spheres in the *in situ* SAXS studies. Firstly, the BzMA-swollen PSMA₃₁-PBzMA_x spheres were heated at 90 °C for 1 h and then centrifuged at 13,000 rpm for 1 to 10 h at 20 °C to ensure

complete sedimentation of the spheres. Since centrifugation was not possible at 90 °C, it is assumed that the amount of BzMA monomer within the PBzMA cores is the same at 20 °C and 90 °C. Each supernatant was then analyzed for its BzMA content against an internal standard (triethoxymethylsilane) via ^1H NMR spectroscopy (see Supporting Information for further details). The experimentally-determined values of φ_{BzMA} at particular BzMA conversions were then fitted to a logarithmic decay function ($R^2 > 0.95$), which was subsequently utilized to calculate φ_{BzMA} values for all entries in Table 1 via interpolation. Equation 1 was then used to calculate the corresponding N_s values. According to the SAXS fittings, the uncertainty in R_s is small, hence the error in N_s is dominated by that associated with V_s , which is in turn dictated by the molecular weight distribution (MWD) of the growing core-forming PBzMA block. Given that the PSMA₃₁ stabilizer block is relatively short, this MWD is approximately the same as that of the diblock copolymer. However, since the *in situ* SAXS experiments were conducted on such a small scale, it was not feasible to determine the copolymer MWD at intermediate times during the polymerization. Therefore, the maximum error in V_s at any given time during the polymerization was estimated from the final MWD obtained for the laboratory-scale synthesis of the equivalent PSMA₃₁-PBzMA₂₀₀₀ spheres. The unimodal MWD determined by THF GPC was fitted to a Gaussian model to determine its standard deviation (see Supporting Information), which was found to be approximately 9.5%. Since the PISA synthesis conducted under *in situ* SAXS conditions proceeded much faster than standard laboratory conditions, it is possible that a broader MWD is observed for the copolymers synthesized in the former case. However, several recent reports of PISA syntheses conducted in non-polar solvents indicate that there is no correlation between copolymer MWD and the final copolymer morphology – even highly polydisperse copolymer chains ($M_w/M_n > 2.0$) can self-assemble to give well-defined nano-objects.^{85, 86}

N_s gradually increased with polymerization time, as indicated in Figure 5b (black data). This is not unexpected in view of recent observations made by both Jones *et al.*⁷⁰ and Zhang and co-workers⁸⁷ for non-aqueous PISA formulations. Nevertheless, it provides the first direct experimental evidence that the mean number of copolymer chains per nanoparticle increases during PISA syntheses. Likely mechanisms are either efficient fusion between monomer-swollen spheres and/or continuous aggregation of molecularly-dissolved copolymer chains.⁷⁰ The latter seems more likely to occur during the early stages of the polymerization (just after nucleation), rather than in the latter stages. The average number of copolymer chains per unit surface area (S_{agg}) during the polymerization was calculated using Equation 2 below.

$$S_{\text{agg}} = \frac{N_s}{4\pi R_s^2} \quad (2)$$

Interestingly, S_{agg} values (Figure 5b, red data) decrease from 0.075 nm⁻² to a limiting value of approximately 0.04 nm⁻² after around 40 min, suggesting an optimum surface packing density

of copolymer chains within the sterically-stabilized PSMA₃₁-PBzMA₂₀₀₀ spherical nanoparticles.⁷⁰

The average distance between adjacent chains at the core-shell interface (d_{int}) was calculated using Equation 3 below.⁷⁶

$$d_{\text{int}} = \sqrt{\frac{4\pi R_s^2}{N_s}} = \sqrt{\frac{1}{S_{\text{agg}}}} \quad (3)$$

For small spheres (i.e., $D_s = 35.4$ nm), d_{int} was calculated to be 3.67 nm after 8 min (or 5.0% BzMA conversion, which corresponds to PSMA₃₁-PBzMA₉₉). This is comparable to that reported by Förster *et al.*⁷⁶ for similar-sized polystyrene-poly(4-vinyl pyridine) block copolymer micelles, for which d_{int} was found to be 3.20 nm. Subsequently, d_{int} increased up to 5.04 nm at full conversion (i.e., PSMA₃₁-PBzMA₂₀₀₀; $D_s = 116.9$ nm), indicating that copolymer chains with longer core-forming PBzMA blocks occupy a larger surface area at the core-shell interface.

PSMA₁₃-PBzMA_x block copolymer syntheses and corresponding phase diagram

Utilizing a shorter PSMA₁₃ macro-CTA to target PBzMA core-forming block DPs of 20 to 150 at various copolymer concentrations enabled access to spherical, worm-like and vesicular morphologies at relatively low copolymer concentrations (≥ 5 % w/w solids). In contrast, well-defined vesicular morphologies were only obtained at copolymer concentrations of at least 12.5% w/w solids for the PISA synthesis of PLMA-PBzMA diblock copolymer nanoparticles, whereas somewhat higher copolymer concentrations ($\geq 17.5\%$ w/w solids) were required to access a pure worm phase.^{28, 57, 58} A detailed phase diagram was constructed for the present PSMA₁₃-PBzMA_x formulation, with diblock copolymer morphologies assigned via *post mortem* TEM studies (see Figure 6). Such phase diagrams are essential to ensure reproducible targeting of the desired copolymer morphology. Thus spheres were obtained at all copolymer concentrations investigated (5-20% w/w) when targeting PBzMA block DPs of 30 to 50. As reported for related PISA formulations,^{26, 28, 34, 45, 46, 57, 58, 62} the worm phase space is relatively narrow and is bounded by mixed phase regions. As expected, pure vesicles were obtained by targeting asymmetric PSMA₁₃-PBzMA_x diblock copolymers (i.e. $x > 80$). However, for PBzMA DPs of up to 150 this phase appears to be confined to copolymer concentrations of 5-15% w/w solids, with mixed phases being obtained at 20% w/w solids. It is perhaps worth emphasizing that the ability to prepare vesicles at copolymer concentrations as low as 5% w/w solids is an important advantage for *in situ* SAXS studies (see later). This is because lower copolymer concentrations minimize structural effects arising from inter-particle interactions.

Post mortem SAXS patterns recorded for 1.0% w/w dispersions of eight PSMA₁₃-PBzMA_x diblock copolymer nano-objects (originally prepared at 10% w/w solids; see phase diagram in Figure 6) are depicted in Figure 7. Each of the three examples of spherical nanoparticles exhibit an approximate zero gradient at low q , as expected.⁸⁸ Some deviations from

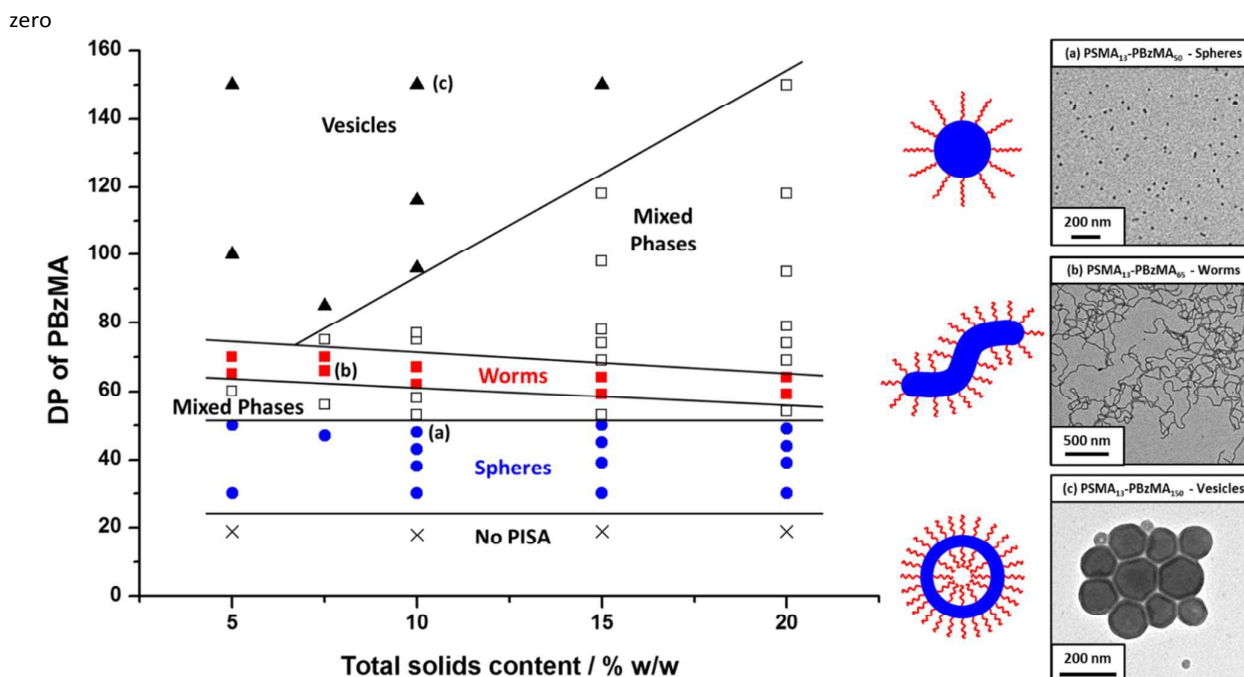


Fig. 6 Phase diagram constructed for PSMA₁₃-PBzMA_x diblock copolymer nanoparticles prepared by RAFT dispersion polymerization of BzMA in mineral oil using a PSMA₁₃ macro-CTA and T21s initiator at 90 °C ([PSMA₁₃]/[T21s] molar ratio = 5.0). The *post mortem* diblock copolymer morphologies obtained at full conversion were assigned on the basis of TEM studies. TEM images (a), (b) and (c) correspond to typical examples of the three pure copolymer morphologies (spheres, worms and vesicles) respectively.

gradient observed at low q values could be associated with an aggregation of the spherical micelles. The local minimum observed for each scattering curve at $q \approx 0.5\text{--}0.7\text{ nm}^{-1}$ gradually shifted to lower q on increasing the mean PBzMA DP from 40 to 50, indicating a progressive increase in the sphere dimensions. This is consistent with previously reported PISA syntheses conducted using a fixed stabilizer block DP, where increasing the core-forming block DP led to larger spherical nanoparticles.^{33, 57} According to theory, rigid rods should exhibit a limiting gradient of -1 at low q .⁸⁸ However, TEM studies (see Figure 6b) suggest that these particular worms exhibit appreciable flexibility. Nevertheless, the SAXS patterns recorded for PSMA₁₃-PBzMA₆₅ and PSMA₁₃-PBzMA₇₀ worms in Figure 7 do indeed exhibit gradients of approximately -1 at low q . For these two copolymer dispersions, the local minimum observed at $q \approx 0.5\text{--}0.6\text{ nm}^{-1}$ is associated with the mean worm width. Vesicular morphologies were also confirmed for PSMA₁₃-PBzMA₁₀₀₋₁₅₀, since SAXS patterns indicated a slope of approximately -2 at low q for these three dispersions. For such hollow spheres, there are two characteristic local minima. Firstly, the minimum observed at $q \approx 0.4\text{--}0.6\text{ nm}^{-1}$ is associated with the vesicle membrane thickness (T_m), which increases monotonically as higher PBzMA DPs are targeted. Secondly, the local minimum observed at $q \approx 0.04\text{--}0.05\text{ nm}^{-1}$ is characteristic of the overall vesicle dimensions. Interestingly, this parameter remains relatively constant ($109 \pm 5\text{ nm}$) for the series of three PSMA₁₃-PBzMA₁₀₀₋₁₅₀ vesicles prepared at 10% w/w solids shown in Figure 6.

In situ SAXS studies of the PISA synthesis of PSMA₁₃-PBzMA₁₅₀ vesicles

A series of *in situ* SAXS patterns were also recorded when targeting PSMA₁₃-PBzMA₁₅₀ vesicles at 10% w/w solids in mineral oil. This core-forming block DP was chosen to guarantee access vesicle space (see Figure 6) while maximizing the time scales for the existence of the intermediate sphere and worm phases. Inspecting Figure 8, this strategy was clearly successful since the full range of copolymer morphologies is observed, from initially soluble copolymer chains through to the final vesicular morphology via intermediate spherical and worm-like nanoparticles.³⁵ Again, the polymerization kinetics required renormalization prior to detailed data analyses (see Figure S4). In this case, a significantly longer polymerization time (and hence a somewhat higher BzMA conversion) is required for the onset of micellization. Inspecting Figure 6, it is clear that the critical DP for the core-forming PBzMA block required to induce nucleation is around 30. This is because PSMA₁₃-PBzMA₂₀ diblock copolymers do not self-assemble in mineral oil at 90 °C, whereas PSMA₁₃-PBzMA₃₀ diblock copolymer spheres are observed under these conditions. Thus approximately 20% BzMA conversion is required to trigger *in situ* self-assembly for this particular PSMA₁₃-PBzMA₁₅₀ PISA formulation. In contrast, when targeting PSMA₃₁-PBzMA₂₀₀₀ diblock copolymer spheres (Figure 3), a BzMA conversion of only $\sim 1.5\%$ is required to achieve the same critical PBzMA DP for micellar nucleation. Spherical nanoparticles are formed just after the onset of micellization, as confirmed by the approximately zero gradient at low q .⁸⁸ However, just 10 min after nucleation this low q gradient tends towards -1 , indicating that the nascent spherical nanoparticles undergo multiple 1D fusion events leading to the formation of highly anisotropic worms. This second morphology

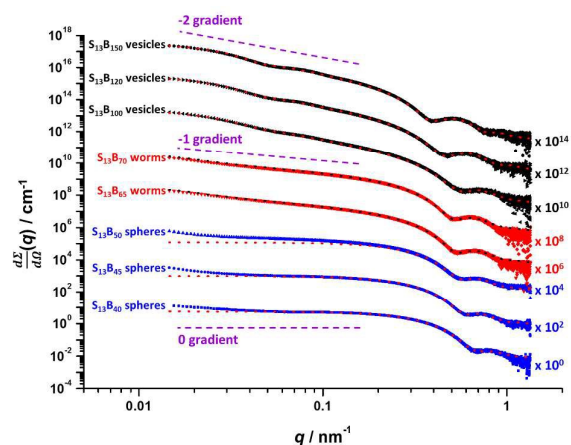


Fig. 7 Small angle X-ray scattering (SAXS) patterns and data fits (dashed lines) for 1.0% w/w dispersions of PSMA₁₃-PBzMA_x (denoted as S₁₃-B_x for brevity) diblock copolymer nanoparticles synthesized via RAFT dispersion polymerization of BzMA at 10% w/w solids in mineral oil. Purple dashed lines indicate zero, -1 and -2 gradients for guidance.

is relatively short-lived (~6 min), which is consistent with the narrow worm phase space observed in the phase diagram (Figure 6). A mixed phase of worms and vesicles is apparent from 46 to 56 min. This corresponds to a PBzMA DP of 76 to 104 and is consistent with the mixed phase region observed in Figure 6. Informed by these *in situ* studies, multiple aliquots were taken from the same polymerization conducted under standard laboratory conditions, with particular attention being paid to the above DP interval. TEM analyses confirmed that vesicles are formed from worms via octopi (see Figure S7b) and jellyfish (see Figures S5c and S5d) intermediates. Such transient structures were also reported by Blanazs and co-workers³⁵ for an aqueous PISA formulation when targeting vesicles as the final copolymer morphology. This provides the first evidence of octopi and jellyfish intermediates for a non-polar PISA formulation and suggests that the worm-to-vesicle morphology transition via such structures is likely to be universal for all vesicles prepared via PISA syntheses. Finally, well-defined vesicles are present as a pure phase in the latter stages of the polymerization (~58-120 min), as indicated by the slope of -2 at low q .

For this particular *in situ* SAXS study (see Figure 8), the experimental protocol used to renormalize the polymerization kinetics can be validated by comparing the PBzMA DP ranges within which pure spheres, worms and vesicles are observed to those indicated within the phase diagram shown in Figure 6 (see Table 2). The generally good agreement between the upper and lower DPs at which each pure morphology is observed provides strong evidence that the analytical approach employed to renormalize the kinetic data is indeed valid. It is also worth emphasizing that the relatively well-defined phase boundaries shown in Figure 6 enable a particularly robust comparison. SAXS patterns assigned to pure vesicles exhibit two local minima: one is a rather subtle feature at $q \approx 0.04$ - 0.07 nm^{-1} representing the overall vesicle dimensions and the other is a more pronounced feature at $q \approx 0.3$ - 0.7 nm^{-1} that is associated with the vesicle membrane thickness (T_m).⁶⁷ Figure 9a shows selected SAXS patterns taken from Figure 8 over a much narrower q range in

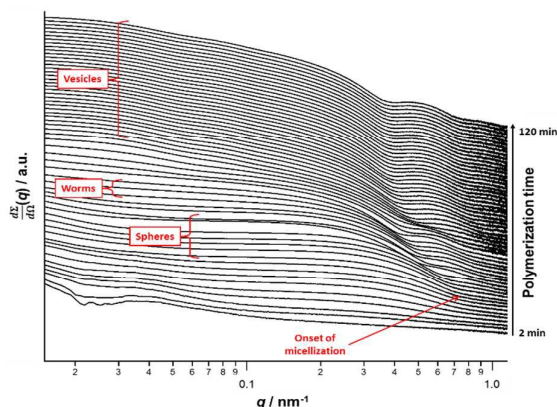


Fig. 8 *In situ* SAXS patterns recorded for the PISA synthesis of PSMA₁₃-PBzMA₁₅₀ diblock copolymer vesicles prepared at 90 °C in mineral oil at 10% w/w solids. The onset of micellar nucleation is indicated by the red arrow.

Table 2 Comparison of the lower and upper limit PBzMA DPs for the three pure copolymer morphologies (spheres, worms and vesicles) determined by (i) inspecting the phase diagram constructed for PSMA₁₃-PBzMA_x diblock copolymer nanoparticles (Figure 6) and (ii) *in situ* SAXS analysis of the synthesis of PSMA₁₃-PBzMA₁₅₀ vesicles (Figure 8).

Pure copolymer morphology		PBzMA DP indicated by phase diagram	PBzMA DP indicated by <i>in situ</i> SAXS studies
Spheres	Lower limit bound	25 ± 5	29 ± 3
	Upper limit bound	51 ± 1	48 ± 4
Worms	Lower limit bound	60 ± 1	59 ± 5
	Upper limit bound	70 ± 1	70 ± 6
Vesicles	Lower limit bound	93 ± 2	108 ± 4

order to better illustrate the evolution in T_m at $q \approx 0.3$ - 0.7 nm^{-1} . A pure vesicle phase is observed after 58 min, with subsequent data fits indicating that T_m increases monotonically from 10.3 nm to 14.1 nm for PBzMA DPs ranging from 108 to 150 (see Figure 9b, red data and Table 3). There is also an apparent increase in the outer core radius (R_{out}) with increasing PBzMA DP (see Table 3) but this rather modest increase appears to be within the relatively large error associated with these data.

Precise knowledge of the dimensions of the growing vesicles is important, because in principle this enables the vesicle growth mechanism to be deduced. For example, Warren *et al.*⁶⁷ reported that the overall diameter of poly(glycerol monomethacrylate)-poly(2-hydroxypropyl methacrylate) (PGMA-PPMA) vesicles prepared via aqueous RAFT dispersion polymerization remained constant while T_m increased when targeting higher PHPMA DPs. This indicates that the constrained vesicles grow inwards, with the thickening membrane leading to a reduction in the vesicle lumen volume. In order to elucidate the growth mechanism for the PSMA₁₃-PBzMA_x vesicles described in this work, much higher PBzMA DPs must be targeted. Consequently, PSMA₁₃-PBzMA_x vesicles with PBzMA

Table 3. Evolution of the BzMA conversion, mean degree of polymerization (DP) for the core-forming PBzMA block, molecular volume of a single PBzMA core-forming block within the membrane (V_m), outer core radius (R_{out}), membrane thickness (T_m) and inner core radius ($R_{in} = R_{out} - T_m$) during the PISA synthesis of PSMA₁₃-PBzMA₁₅₀ diblock copolymer vesicles. The associated error in V_m is indicated and the standard deviation is shown where relevant ($\pm \sigma_{R_{out}}, \sigma_{T_m}, \sigma_{R_{in}}$).

Time / min	BzMA Conversion / %	PBzMA DP	V_m / nm^3	R_{out} / nm	T_m / nm	R_{in} / nm
58	72.3	108	27 ± 0.9	53 ± 18	10 ± 1.6	43 ± 18
60	75.4	113	28 ± 1.0	56 ± 19	11 ± 1.6	45 ± 19
62	78.2	117	29 ± 1.0	56 ± 19	11 ± 1.6	45 ± 19
64	80.7	122	30 ± 1.0	56 ± 19	12 ± 1.6	44 ± 19
68	85.2	128	32 ± 1.1	57 ± 20	12 ± 1.8	45 ± 20
72	88.9	134	33 ± 1.1	57 ± 20	13 ± 1.8	44 ± 20
76	91.8	138	34 ± 1.2	57 ± 19	13 ± 1.9	44 ± 19
88	97.1	146	36 ± 1.2	57 ± 20	14 ± 2.0	44 ± 20
120	100	150	37 ± 1.3	59 ± 20	14 ± 2.2	45 ± 21

DPs up to 2000 (prepared at 10% w/w solids on a 5.0 mL scale) were subjected to *post mortem* analysis using DLS, TEM and SAXS (see Supporting Information). DLS studies indicated that the overall vesicle diameter remained essentially constant (140-145 nm) for PBzMA DPs of between 100 and 400 (see Figure 9c, blue data). For reference, the corresponding SAXS data reported in Table 3 for the *in situ* SAXS studies are also shown in Figure 9c. The apparent discrepancy between these two data sets simply reflects the intensity-average and volume-average vesicle diameters reported by DLS and SAXS respectively. DLS diameters systematically increased for PBzMA DPs between 500 and 2000, while the corresponding size distributions significantly broadened for PBzMA DPs above 900. These data suggest that the vesicles become unstable for PBzMA DPs greater than 400, as similarly reported by Warren *et al.* for PGMA-PPHMA vesicles.⁶⁷ TEM studies (see Figure S8a) support these DLS data: vesicles with narrow size distributions and approximately constant diameters were observed for PBzMA DPs up to 400. This indicates that the *apparent* increase in overall vesicle dimensions observed in the *in situ* SAXS studies (see Table 3) is actually an artefact. Moreover, the vesicle membrane thickness increases with PBzMA DP over this range, which suggests a similar 'inward growth' mechanism. Importantly, there is excellent agreement between the *in situ* and *post mortem* T_m data sets shown in Figure 9b, which further supports the validity of our kinetics renormalization approach. Furthermore, large, ill-defined species are observed for PBzMA DPs above 500 (see vertical dashed line in Figure 9c). This is consistent with observations made by Warren *et al.*,⁶⁷ who reported loss of the vesicular morphology for PPHMA DPs above 1000. In view of these observations, further *post mortem* SAXS studies were undertaken to monitor the evolution of the PSMA₁₃-PBzMA_x morphology (see red data set in Figure 9c and also Figure S8b). It should be noted that these additional SAXS measurements were performed using an in-house NanoStar instrument, rather than a synchrotron X-ray source. Thus the accessible q range was only sufficient to allow the evolution in T_m to be monitored – no information regarding the overall vesicle dimensions could be obtained. T_m increased monotonically from 9 nm to 30 nm on increasing the target PBzMA DP from

100 to 400. The data were fitted to the power law $T_m = k \cdot x^\alpha$ where k is a constant and x is the PBzMA DP. The α exponent was calculated to be 0.86, which is consistent with that reported by Warren *et al.*⁶⁷ via *post mortem* SAXS analysis of PGMA-PPHMA vesicles ($\alpha = 0.79$). For PBzMA DPs above 400, the T_m feature at around $q = 0.2 \text{ nm}^{-1}$ to 0.6 nm^{-1} becomes increasingly indistinct. This indicates the gradual loss of the vesicular morphology, which is consistent with the corresponding TEM studies. Since the DLS data indicate approximately the same overall vesicle dimensions for PBzMA DPs of 100-400, this indicates that the 'inward growth' mechanism is valid for both aqueous and non-polar media (see Figure 9d). This is important, because it implies a *generic* vesicle growth mechanism for all PISA formulations. This is perfectly reasonable, because Warren *et al.* showed that this hitherto unrecognized mechanism is the *only* means by which the vesicles can lower their total surface area, and hence reduce their overall free energy.⁶⁷

In the case of vesicles, different equations are required for the calculation of mean aggregation number per vesicle (N_v), S_{agg} and d_{int} , as indicated below (see Equations 4, 5 and 6). By definition, the volume fraction of BzMA *monomer* within the core domain (ϕ_{BzMA}) at full conversion must be zero. Moreover, the SAXS data fits suggest that the volume fraction of *solvent* within the PBzMA chains forming the vesicle membrane (x_{sol}) is close to zero. In this case, N_v for the final PSMA₁₃-PBzMA₁₅₀ vesicles can be calculated using Equation 4 below.

$$N_v = \frac{\frac{4}{3}\pi(R_{out}^3 - R_{in}^3)}{V_m} \quad (4)$$

As for the earlier *in situ* SAXS studies conducted when targeting PSMA₃₁-PBzMA₂₀₀₀ spheres, the leading error in the calculation of N_v is the MWD of the core-forming PBzMA block, which dictates the error in V_m . From the GPC data obtained for PSMA₁₃-PBzMA₁₅₀ vesicles prepared on a laboratory scale, the standard deviation in V_m was estimated to be 3.4% using the same method used for the spheres (see Supporting Information). S_{agg} and d_{int} for the PSMA₁₃-PBzMA₁₅₀ vesicles are subsequently calculated using Equations 5 and 6, respectively.

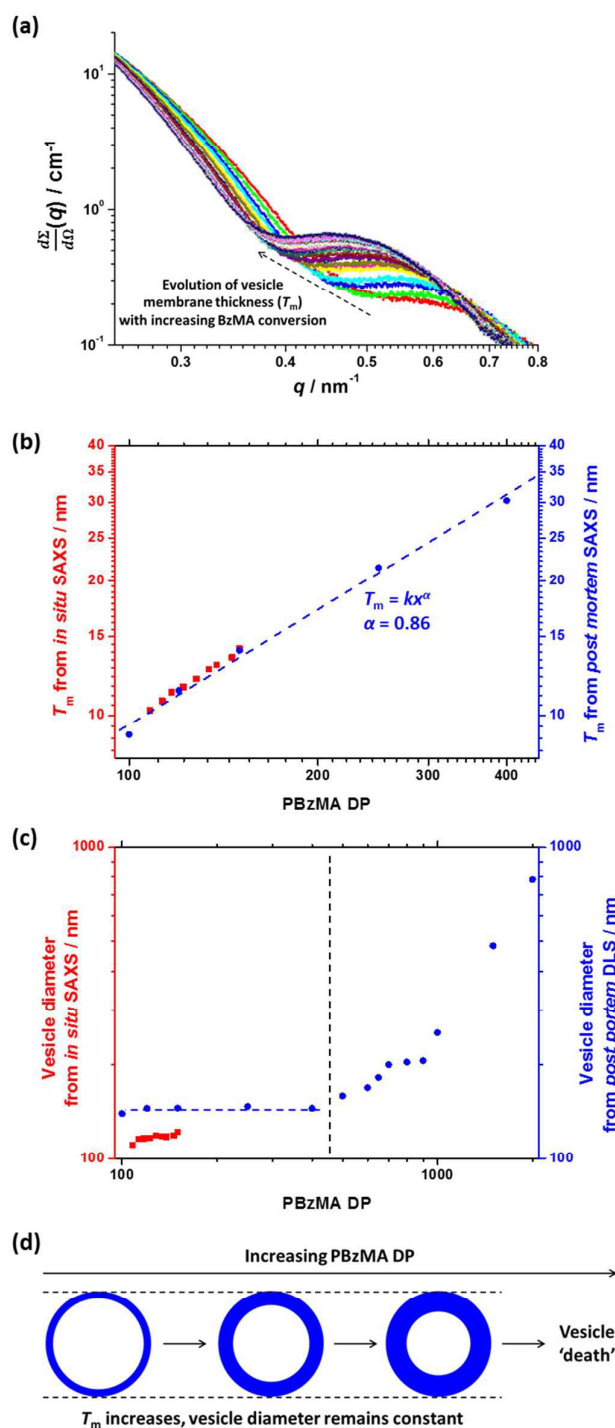


Figure 9. (a) *In situ* SAXS patterns showing the evolution of the vesicular membrane thickness (T_m). (b) The relationship between T_m and PBzMA DP and judged by *in situ* SAXS when targeting PSMA₁₃-PBzMA₁₅₀ vesicles (red squares) and *post mortem* SAXS studies of PSMA₁₃-PBzMA_x vesicles (blue circles). (c) Vesicle diameter as judged by *in situ* SAXS when targeting PSMA₁₃-PBzMA_x vesicles (red squares) and *post mortem* DLS studies of PSMA₁₃-PBzMA_x vesicles (blue data). (d) T_m increases monotonically when targeting higher PBzMA DPs while the overall vesicle diameter remains relatively constant, thus the lumen volume is gradually reduced during inward vesicle growth until vesicle 'death' occurs.

$$S_{\text{agg}} = \frac{N_v}{4\pi(R_{\text{out}}^2 + R_{\text{in}}^2)} \quad (5)$$

$$d_{\text{int}} = \sqrt{\frac{4\pi(R_{\text{out}}^2 + R_{\text{in}}^2)}{N_v}} = \sqrt{\frac{1}{S_{\text{agg}}}} \quad (6)$$

The N_v value calculated for PSMA₁₃-PBzMA₁₅₀ vesicles at full conversion was $12\,709 \pm 432$, with the corresponding S_{agg} determined to be $0.187 \pm 0.006 \text{ nm}^{-2}$ and the average distance between adjacent copolymer chains at the core-shell interface (d_{int}) was $2.31 \pm 0.08 \text{ nm}$. These data are somewhat different to those calculated for related aqueous⁶⁷ and alcoholic⁴⁸ PISA formulations, where d_{int} is (retrospectively) calculated to be 3.1–3.4 nm. However, the solvent volume fraction within the vesicle membrane was found to be more than 0.35 in these earlier literature examples compared to zero in the present work. This suggests that the copolymer chains are more densely packed in the current non-polar PISA formulation. Notably, the value of d_{int} calculated for these vesicles is comparable to that determined for densely-packed polybutadiene-poly(L-lysine) block copolymer chains within vesicle membranes formed in saline solution ($d_{\text{int}} = 2.4 \text{ nm}$ at pH 10.3).⁸⁹ The S_{agg} and d_{int} values calculated for PSMA₁₃-PBzMA₁₅₀ vesicles can also be compared to those for PSMA₃₁-PBzMA₂₀₀₀ spheres ($S_{\text{agg}} = 0.039 \pm 0.004 \text{ nm}^{-2}$, $d_{\text{int}} = 5.04 \pm 0.48 \text{ nm}$). It is evident that the copolymer chains are packed more densely within the PSMA₁₃-PBzMA₁₅₀ vesicles compared to the PSMA₃₁-PBzMA₂₀₀₀ spheres. This is likely to be the result of the differing interfacial curvatures associated with each copolymer morphology, but the significant difference in target DP for the core-forming PBzMA blocks may also be a factor.

Conclusions

In summary, a range of sterically-stabilized PSMA-PBzMA diblock copolymer nano-objects have been prepared via RAFT dispersion polymerization in mineral oil. Improved control over the copolymer molecular weight distribution is achieved compared to previously reported PISA syntheses conducted in non-polar media, with relatively narrow molecular weight distributions ($M_w/M_n \leq 1.30$) being achieved even when targeting PBzMA DPs of up to 500. As expected, only spherical nanoparticles were obtained when using relatively long PSMA₁₈ or PSMA₃₁ macro-CTAs. In both cases, a clear correlation was observed between the mean sphere diameter (as judged by DLS) and the core-forming PBzMA DP. PSMA₃₁-PBzMA_x spheres indicated a scaling exponent of 0.50, suggesting essentially non-solvated PBzMA chains within the core-forming PBzMA block, whereas a scaling exponent of 0.61 was obtained for PSMA₁₈-PBzMA_x spheres, suggesting a finite degree of solvation for the PBzMA chains in this case. In contrast, using a relatively short PSMA₁₃ macro-CTA allows the synthesis of spherical, worm-like or vesicular morphologies. Construction of a detailed phase diagram for PSMA₁₃-PBzMA_x diblock copolymers confirmed that pure spheres, worms or vesicles could be obtained at relatively low solids concentrations. This is important, because in principle it

facilitates *in situ* SAXS studies of the formation of PSMA₃₁-PBzMA₂₀₀₀ spheres and PSMA₁₃-PBzMA₁₅₀ nano-objects at 10% w/w solids. However, the rate of BzMA polymerization during such scattering experiments is significantly faster than that observed under normal laboratory conditions. Thus the latter kinetic data sets require renormalization to enable detailed analysis of the *in situ* SAXS data. When targeting PSMA₃₁-PBzMA₂₀₀₀ spheres, a systematic increase in core diameter (D_c) and mean aggregation number (N_s) are clearly discernible during the BzMA polymerization, with the final scattering pattern indicating the formation of near-monodisperse PSMA₃₁-PBzMA₂₀₀₀ spheres. Interestingly, the number of copolymer chains per unit surface area (S_{agg}) decreased rapidly during the initial stages of the polymerization until a limiting value of $\sim 0.038 \text{ nm}^{-2}$ is attained. This indicated that the mean distance between copolymer chains at the core-shell interface (d_{int}) at full conversion was approximately 5.0 nm. When targeting PSMA₁₃-PBzMA₁₅₀ vesicles, characteristic scattering patterns for the dissolved copolymer chains, intermediate spheres and worms, and the final vesicle morphology were obtained. Importantly, revisiting the phase diagram constructed for this formulation enabled validation of the renormalization protocol adopted for the kinetic data. More specifically, the mean PBzMA DPs corresponding to the various phase boundaries were in relatively good agreement with those DPs assigned to the corresponding pure phases indicated by analysis of the *in situ* SAXS patterns. Within the mixed phase space, it was shown that vesicles are formed from worms via octopi and jellyfish intermediates as first reported for an aqueous PISA formulation. Combined DLS, TEM and SAXS studies indicate that the overall vesicle dimensions remain relatively constant as the vesicle membrane gradually thickens with increasing PBzMA DP until so-called vesicle 'death' occurs.

These observations indicate an 'inward growth' mechanism, as recently reported for an aqueous PISA formulation. This suggests a *generic* vesicle growth mechanism is most likely applicable for such syntheses.

Acknowledgements

We are grateful to Diamond Light Source for providing synchrotron beam time and thank the personnel of I22 for their assistance. Lubrizol Corporation Ltd is thanked for funding a PhD studentship for MJD. EPSRC is thanked for a Platform grant (EP/J007846/1) to support LAF, OOM, NJW and SPA also acknowledges an ERC Advanced Investigator grant (PISA 320372) supporting both himself and CJM.

Notes and references

1. S. Krause, *Journal of Physical Chemistry*, 1964, **68**, 1948-1955.
2. Z. Tuzar and P. Kratochvil, *Advances in Colloid and Interface Science*, 1976, **6**, 201-232.
3. R. K. O'Reilly, C. J. Hawker and K. L. Wooley, *Chemical Society Reviews*, 2006, **35**, 1068-1083.
4. M. Antonietti and S. Förster, *Advanced Materials*, 2003, **15**, 1323-1333.
5. L. J. M. Vagberg, K. A. Cogan and A. P. Gast, *Macromolecules*, 1991, **24**, 1670-1677.
6. L. F. Zhang and A. Eisenberg, *Science*, 1995, **268**, 1728-1731.
7. G. Mountrichas, M. Mpiri and S. Pispas, *Macromolecules*, 2005, **38**, 940-947.
8. S. Y. Choi, F. S. Bates and T. P. Lodge, *Journal of Physical Chemistry B*, 2009, **113**, 13840-13848.
9. J. Tao, S. Stewart, G. J. Liu and M. L. Yang, *Macromolecules*, 1997, **30**, 2738-2745.
10. G. J. Liu, J. F. Ding, L. J. Qiao, A. Guo, B. P. Dymov, J. T. Gleeson, T. Hashimoto and K. Saijo, *Chemistry-a European Journal*, 1999, **5**, 2740-2749.
11. N. Ouarti, P. Viville, R. Lazzaroni, E. Minatti, M. Schappacher, A. Deffieux and R. Borsali, *Langmuir*, 2005, **21**, 1180-1186.
12. M. Lazzari, D. Scalarone, C. Vazquez-Vazquez and M. A. Lopez-Quintela, *Macromolecular Rapid Communications*, 2008, **29**, 352-357.
13. J. B. Gilroy, T. Gadt, G. R. Whittell, L. Chabanne, J. M. Mitchels, R. M. Richardson, M. A. Winnik and I. Manners, *Nature Chemistry*, 2010, **2**, 566-570.
14. J. A. Massey, K. Temple, L. Cao, Y. Rharbi, J. Raez, M. A. Winnik and I. Manners, *Journal of the American Chemical Society*, 2000, **122**, 11577-11584.
15. X. Wang, G. Guerin, H. Wang, Y. Wang, I. Manners and M. A. Winnik, *Science*, 2007, **317**, 644-647.
16. T. Gaedt, N. S. Jeong, G. Cambridge, M. A. Winnik and I. Manners, *Nature Materials*, 2009, **8**, 144-150.
17. R. Zheng, G. Liu, M. Devlin, K. Hux and T.-C. Jao, *Tribology Transactions*, 2010, **53**, 97-107.
18. D. J. Gowney, O. O. Mykhaylyk and S. P. Armes, *Langmuir*, 2014, **30**, 6047-6056.
19. D. J. Gowney, O. O. Mykhaylyk, L. Middlemiss, L. A. Fielding, M. J. Derry, N. Aragrag, G. D. Lamb and S. P. Armes, *Langmuir*, 2015, **31**, 10358-10369.
20. J. Chiefari, Y. K. Chong, F. Ercole, J. Krstina, J. Jeffery, T. P. T. Le, R. T. A. Mayadunne, G. F. Meijs, C. L. Moad, G. Moad, E. Rizzardo and S. H. Thang, *Macromolecules*, 1998, **31**, 5559-5562.
21. G. Moad, E. Rizzardo and S. H. Thang, *Australian Journal of Chemistry*, 2005, **58**, 379-410.
22. G. Moad, E. Rizzardo and S. H. Thang, *Accounts of Chemical Research*, 2008, **41**, 1133-1142.
23. B. Charleux, G. Delaittre, J. Rieger and F. D'Agosto, *Macromolecules*, 2012, **45**, 6753-6765.
24. M. J. Monteiro and M. F. Cunningham, *Macromolecules*, 2012, **45**, 4939-4957.
25. J.-T. Sun, C.-Y. Hong and C.-Y. Pan, *Polymer Chemistry*, 2013, **4**, 873-881.
26. N. J. Warren and S. P. Armes, *Journal of the American Chemical Society*, 2014, **136**, 10174-10185.
27. M. J. Derry, L. A. Fielding and S. P. Armes, *Progress in Polymer Science*, 2016, **52**, 1-18.
28. M. J. Derry, L. A. Fielding and S. P. Armes, *Polymer Chemistry*, 2015, **6**, 3054-3062.
29. Z. An, Q. Shi, W. Tang, C.-K. Tsung, C. J. Hawker and G. D. Stucky, *Journal of the American Chemical Society*, 2007, **129**, 14493-14499.

30. A. Blanazs, S. P. Armes and A. J. Ryan, *Macromolecular Rapid Communications*, 2009, **30**, 267-277.
31. J. Rieger, C. Grazon, B. Charleux, D. Alaimo and C. Jérôme, *Journal of Polymer Science Part A: Polymer Chemistry*, 2009, **47**, 2373-2390.
32. S. Boisse, J. Rieger, K. Belal, A. Di-Cicco, P. Beaunier, M.-H. Li and B. Charleux, *Chemical Communications*, 2010, **46**, 1950-1952.
33. Y. Li and S. P. Armes, *Angewandte Chemie-International Edition*, 2010, **49**, 4042-4046.
34. S. Sugihara, A. Blanazs, S. P. Armes, A. J. Ryan and A. L. Lewis, *Journal of the American Chemical Society*, 2011, **133**, 15707-15713.
35. A. Blanazs, J. Madsen, G. Battaglia, A. J. Ryan and S. P. Armes, *Journal of the American Chemical Society*, 2011, **133**, 16581-16587.
36. G. Liu, Q. Qiu, W. Shen and Z. An, *Macromolecules*, 2011, **44**, 5237-5245.
37. A. Blanazs, A. J. Ryan and S. P. Armes, *Macromolecules*, 2012, **45**, 5099-5107.
38. N. J. Warren, O. O. Mykhaylyk, D. Mahmood, A. J. Ryan and S. P. Armes, *Journal of the American Chemical Society*, 2014, **136**, 1023-1033.
39. C. A. Figg, A. Simula, K. A. Gebre, B. S. Tucker, D. M. Haddleton and B. S. Sumerlin, *Chemical Science*, 2015, **6**, 1230-1236.
40. J. Tan, H. Sun, M. Yu, B. S. Sumerlin and L. Zhang, *ACS Macro Letters*, 2015, **4**, 1249-1253.
41. W.-M. Wan and C.-Y. Pan, *Polymer Chemistry*, 2010, **1**, 1475-1484.
42. W.-M. Wan, X.-L. Sun and C.-Y. Pan, *Macromolecular Rapid Communications*, 2010, **31**, 399-404.
43. W. Cai, W. Wan, C. Hong, C. Huang and C. Pan, *Soft Matter*, 2010, **6**, 5554-5561.
44. C.-Q. Huang and C.-Y. Pan, *Polymer*, 2010, **51**, 5115-5121.
45. E. R. Jones, M. Semsarilar, A. Blanazs and S. P. Armes, *Macromolecules*, 2012, **45**, 5091-5098.
46. M. Semsarilar, E. R. Jones, A. Blanazs and S. P. Armes, *Advanced Materials*, 2012, **24**, 3378-3382.
47. M. Semsarilar, E. R. Jones and S. P. Armes, *Polymer Chemistry*, 2014, **5**, 195-203.
48. C. Gonzato, M. Semsarilar, E. R. Jones, F. Li, G. J. P. Krooshof, P. Wyman, O. O. Mykhaylyk, R. Tuinier and S. P. Armes, *Journal of the American Chemical Society*, 2014, **136**, 11100-11106.
49. Y. Pei and A. B. Lowe, *Polymer Chemistry*, 2014, **5**, 2342-2351.
50. Y. W. Pei, N. C. Dharsana, J. A. Van Hensbergen, R. P. Burford, P. J. Roth and A. B. Lowe, *Soft Matter*, 2014, **10**, 5787-5796.
51. B. Karagoz, C. Boyer and T. P. Davis, *Macromolecular Rapid Communications*, 2014, **35**, 417-421.
52. B. Karagoz, L. Esser, H. T. Duong, J. S. Basuki, C. Boyer and T. P. Davis, *Polymer Chemistry*, 2014, **5**, 350-355.
53. S. Dong, W. Zhao, F. P. Lucien, S. Perrier and P. B. Zetterlund, *Polymer Chemistry*, 2015, **6**, 2249-2254.
54. L. Houillot, C. Bui, M. Save, B. Charleux, C. Farcet, C. Moire, J.-A. Raust and I. Rodriguez, *Macromolecules*, 2007, **40**, 6500-6509.
55. L. Houillot, C. Bui, C. Farcet, C. Moire, J.-A. Raust, H. Pasch, M. Save and B. Charleux, *ACS Applied Materials & Interfaces*, 2010, **2**, 434-442.
56. J. A. Raust, L. Houillot, M. Save, B. Charleux, C. Moire, C. Farcet and H. Pasch, *Macromolecules*, 2010, **43**, 8755-8765.
57. L. A. Fielding, M. J. Derry, V. Ladmiral, J. Rosselgong, A. M. Rodrigues, L. P. D. Ratcliffe, S. Sugihara and S. P. Armes, *Chemical Science*, 2013, **4**, 2081-2087.
58. L. A. Fielding, J. A. Lane, M. J. Derry, O. O. Mykhaylyk and S. P. Armes, *Journal of the American Chemical Society*, 2014, **136**, 5790-5798.
59. Y. Pei, L. Thurairajah, O. R. Sugita and A. B. Lowe, *Macromolecules*, 2015, **48**, 236-244.
60. Y. Pei, J.-M. Noy, P. J. Roth and A. B. Lowe, *Journal of Polymer Science Part A: Polymer Chemistry*, 2015, **53**, 2326-2335.
61. Y. Pei, O. R. Sugita, L. Thurairajah and A. B. Lowe, *RSC Advances*, 2015, **5**, 17636-17646.
62. A. P. Lopez-Oliva, N. J. Warren, A. Rajkumar, O. O. Mykhaylyk, M. J. Derry, K. E. B. Doncom, M. J. Rymaruk and S. P. Armes, *Macromolecules*, 2015, **48**, 3547-3555.
63. A. Blanazs, R. Verber, O. O. Mykhaylyk, A. J. Ryan, J. Z. Heath, C. W. I. Douglas and S. P. Armes, *Journal of the American Chemical Society*, 2012, **134**, 9741-9748.
64. V. J. Cunningham, L. P. D. Ratcliffe, A. Blanazs, N. J. Warren, A. J. Smith, O. O. Mykhaylyk and S. P. Armes, *Polymer Chemistry*, 2014, **5**, 6307-6317.
65. M. K. Kocik, O. O. Mykhaylyk and S. P. Armes, *Soft Matter*, 2014, **10**, 3984-3992.
66. C. J. Mable, N. J. Warren, K. L. Thompson, O. O. Mykhaylyk and S. P. Armes, *Chemical Science*, 2015, **6**, 6179-6188.
67. N. J. Warren, O. O. Mykhaylyk, A. J. Ryan, M. Williams, T. Doussineau, P. Dugourd, R. Antoine, G. Portale and S. P. Armes, *Journal of the American Chemical Society*, 2015, **137**, 1929-1937.
68. Y. Kang, A. Pitto-Barry, H. Willcock, W. D. Quan, N. Kirby, A. M. Sanchez and R. K. O'Reilly, *Polymer Chemistry*, 2015, **6**, 106-117.
69. X. W. Zhang, S. Boisse, C. Bui, P. A. Albouy, A. Brulet, M. H. Li, J. Rieger and B. Charleux, *Soft Matter*, 2012, **8**, 1130-1141.
70. E. R. Jones, O. O. Mykhaylyk, M. Semsarilar, M. Boerakker, P. Wyman and S. P. Armes, *Macromolecules*, 2016, **49**, 172-181.
71. J. Jennings, M. Beija, A. P. Richez, S. D. Cooper, P. E. Mignot, K. J. Thurecht, K. S. Jack and S. M. Howdle, *Journal of the American Chemical Society*, 2012, **134**, 4772-4781.
72. D. Hermida-Merino, G. Portale, P. Fields, R. Wilson, S. P. Bassett, J. Jennings, M. Dellar, C. Gommès, S. M. Howdle, B. C. M. Vrolijk and W. Bras, *Review of Scientific Instruments*, 2014, **85**, 093905.
73. P. Cacioli, D. G. Hawthorne, R. L. Laslett, E. Rizzardo and D. H. Solomon, *Journal of Macromolecular Science-Chemistry*, 1986, **23**, 839-852.
74. M. Rodlert, E. Harth, I. Rees and C. J. Hawker, *Journal of Polymer Science Part A-Polymer Chemistry*, 2000, **38**, 4749-4763.
75. F. S. Bates and G. H. Fredrickson, *Annual Review of Physical Chemistry*, 1990, **41**, 525-557.
76. S. Forster, M. Zisenis, E. Wenz and M. Antonietti, *Journal of Chemical Physics*, 1996, **104**, 9956-9970.
77. J. S. Pedersen and M. C. Gerstenberg, *Macromolecules*, 1996, **29**, 1363-1365.

78. J. S. Pedersen and P. Schurtenberger, *Macromolecules*, 1996, **29**, 7602-7612.
79. J. S. Pedersen, *Journal of Applied Crystallography*, 2000, **33**, 637-640.
80. G. Battaglia and A. J. Ryan, *Journal of the American Chemical Society*, 2005, **127**, 8757-8764.
81. J. S. Pedersen, *Journal of Chemical Physics*, 2001, **114**, 2839-2846.
82. S. J. Tseng, C.-C. Chien, Z.-X. Liao, H.-H. Chen, Y.-D. Kang, C.-L. Wang, Y. Hwu and G. Margaritondo, *Soft Matter*, 2012, **8**, 1420-1427.
83. M. H. Qiao, F. Q. Yan, W. S. Sim, J. F. Deng and G. Q. Xu, *Surface Science*, 2000, **460**, 67-73.
84. M. A. Winnik, R. Lukas, W. F. Chen, P. Furlong and M. D. Croucher, *Makromolekulare Chemie-Macromolecular Symposia*, 1987, **10**, 483-501.
85. V. J. Cunningham, S. P. Armes and O. M. Musa, *Polymer Chemistry*, 2016, **7**, 1882-1891.
86. L. P. D. Ratcliffe, B. E. McKenzie, G. M. D. Le Bouëdec, C. N. Williams, S. L. Brown and S. P. Armes, *Macromolecules*, 2015, **48**, 8594-8607.
87. Y. Su, X. Xiao, S. Li, M. Dan, X. Wang and W. Zhang, *Polymer Chemistry*, 2014, **5**, 578-587.
88. O. Glatter and O. Kratky, *Small-angle X-ray Scattering*, Academic Press: London, 1982.
89. R. Sigel, M. Łosik and H. Schlaad, *Langmuir*, 2007, **23**, 7196-7199.